What Causes Hyperfluorescence: Folding Intermediates or Conformationally Flexible Native States?

John Ervin,* Edgar Larios,†§ Szabolcs Osváth,* Klaus Schulten,*†§ and Martin Gruebele*†‡
Departments of *Chemistry and †Physics, ‡Center for Biophysics and Computational Biology, and §Theoretical Biophysics Group, Beckman Institute for Advanced Science and Technology, University of Illinois at Urbana-Champaign, Illinois 61801, USA

ABSTRACT Hyperfluorescent intensity maxima during protein unfolding titrations are often taken as a sign for a thermodynamic folding intermediate. Here we explore another possibility: that hyperfluorescence could be the signature of a "pretransition" conformationally loosened native state. To model such native states, we study mutants of a fluorescent ubiquitin variant, placing cavities at various distances from the tryptophan fluorophore. We examine the correlation between protein flexibility and enhanced fluorescence intensity by using circular dichroism, fluorescence intensity unfolding titrations, fluorescence anisotropy measurements, and molecular dynamics. Based on experiment and simulation, we propose a simple model for hyperfluorescence in terms of static and dynamic conformational properties of the native state during unfolding. Apomyoglobin denaturant unfolding and phosphoglycerate kinase cold denaturation are discussed as examples. Our results do not preclude the existence of thermodynamic intermediates but do raise caution that by itself, hyperfluorescence during unfolding titrations is not conclusive proof of thermodynamic folding intermediates.

INTRODUCTION

Some small proteins, and often larger ones, are multistate folders. Even when obvious traps, such as incorrect disulfide bridges or prolyl isomers, can be ruled out, kinetic folding intermediates exist in many proteins (Jennings and Wright, 1993; Kim and Baldwin, 1990). In such cases, the free energy surface supports local minima besides the denatured and native states. Transient protein populations can accumulate in these intermediate basins. Their origin may lie in additional barriers to native-like sidechain packing (Khorasanizadeh et al., 1996) or in topological and energetic frustration (Onuchic et al., 1995; Shea et al., 2000). Frustration occurs when nonnative contacts form because native ones are far apart in sequence and require a long time to form (Baker, 2000) or because the nonnative contacts have favorable interaction energy (Shea et al., 2000).

Intermediate basins in the free energy surface can be stabilized by appropriate solvent conditions or by mutations. Thermodynamic intermediates are then populated and observed under steady-state conditions (Kim and Baldwin, 1990). Thermodynamic intermediates may not be exactly identical to kinetic intermediates, but they do provide a picture of the higher energy regions of the free energy surface and can model partially folded protein ensembles en route to the native state (Gruebele, 2002).

Tryptophan fluorescence is often used to follow protein unfolding during denaturant, temperature, pressure, or pH titrations. Fluorescence intensity, lifetime, spectral shift, and anisotropy all may be used to monitor conformational changes (Callis and James, 2001; Chen and Barkley, 1998; Hudson et al., 1999; Ross et al., 1981). Many examples exist where unfolding titrations reveal a peak in the tryptophan fluorescence intensity (Beechem et al., 1995; Kiefhaber and Baldwin, 1995; Missiakas et al., 1990; Postnikova et al., 1991; Sabelko et al., 1998). We will term such peaks "hyperfluorescence," as coined by Missiakas et al. (1990). Hyperfluorescence is usually taken as the signature of a thermodynamic folding intermediate. Sometimes it is the only signature detected to corroborate the intermediate.

What indications must one have from detection techniques to decide whether a folding process is thermodynamically two-state or multistate? Reasonable proof of two-state folding requires several titration curves obtained by different techniques but with identical midpoints (steady-state case) or identical exponential rates measured with several probes (kinetic case) (Gruebele, 1999). Conversely, reasonable proof of multistate folding should require multistep transitions or multiphasic kinetics observed by several different probes. One can thus distinguish those "intermediates," which are only detected by tryptophan fluorescence, and those that are also corroborated by another technique, such as circular dichroism (CD), nuclear magnetic resonance, or small angle x-ray scattering.

When fluorescence is used as the only probe, or when other techniques show two-state behavior in apparent contradiction with fluorescence, alternative explanations are possible for tryptophan hyperfluorescence and other unusual tryptophan fluorescence properties. The most likely explanation is a pretransition increase of native state conformational flexibility. No cooperative transition with a barrier needs to be invoked in this case, and nonfluorescent

Submitted November 20, 2001, and accepted for publication March 15, 2002.

J. Ervin and E. Larios contributed equally to this manuscript.

Address reprint requests to M. Gruebele, Chemistry and Physics, Center for Biophysics and Computational Biology, Beckman Institute for Advanced Science and Technology, University of Illinois at Urbana-Champaign, IL 61801. Tel.: 217-333-1624; Fax: 217-244-3186; E-mail: gruebele@scs.uiuc.edu.

0006-3495/02/07/473/11 $2.00

detection methods are expected to show two-state behavior. As discussed in Experimental Methods and Results, native protein fluorescence is more sensitive to conformational flexibility than other techniques, such as CD. Enhanced conformational flexibility alters the fluorescence properties of fluorophores such as tryptophan by populating new conformational ensembles and by promoting interconversion of conformational substates on a nanosecond time scale (Wu and Brand, 1994).

What could cause such enhanced native state flexibility during unfolding? Two-state protein folding transitions are mesoscopic versions of macroscopic phase transitions. In macroscopic systems, increased fluctuations preceding the transition are well documented (Yeomans, 1992). Heat capacity measurements and pressure denaturation studies of proteins also provide some clues. Protein heat capacities have significant baselines before unfolding occurs, a sign that more degrees of freedom are being sampled as the transition is approached (Gomez et al., 1995; Privalov et al., 1971). The volume decrease associated with unfolding is often preceded by a volume increase of the native state relative to the baseline just before the transition. Increased native state volume could lead to increased native state flexibility (Seemann et al., 2001).

Our alternative explanation for hyperfluorescence predicts a positive correlation between enhanced fluorophore mobility and enhanced fluorescence intensity in native proteins. One should compare several very similar native proteins that differ markedly only in their fluorophore mobility. Native proteins with little fluorophore mobility would serve as models for the fully native state, whereas native proteins with enhanced fluorophore mobility would be models for the pretransition native ensemble. To this end, we have studied mutants of a fluorescent ubiquitin variant by CD, fluorescence intensity, fluorescence depolarization, and full-atom solvated molecular dynamics simulations. Aliphatic side chain deletion mutants were designed to create cavities in the native structure either in contact with or away from the fluorophore. These cavities increase fluorophore mobility without directly altering quenching processes. The results show conclusively that fluorescence intensity increases with enhanced mobility of the fluorophore, by amounts comparable with hyperfluorescence. Pretransition loosening of native structure is thus a viable alternative explanation for nonmonotonic fluorescence intensity during unfolding.

Protein hyperfluorescence is of course not always due to enhanced native mobility; true thermodynamic intermediates can hyperfluoresce for the same reasons that a pretransition native state does. A classic example is the I state formed during low pH denaturation of apomyoglobin (Barrick and Baldwin, 1993). The I state can be observed by multiple spectroscopic techniques. However, one needs to raise a note of caution: thermodynamic (and perhaps even kinetic) intermediates should not be assigned on the basis of nonmonotonic fluorescence changes alone. We will briefly discuss two such cases: the already well-characterized case of apomyoglobin undergoing chaotropic denaturation at near-neutral pH and phosphoglycerate kinase undergoing cold denaturation. These processes are best explained by a pretransition native ensemble.

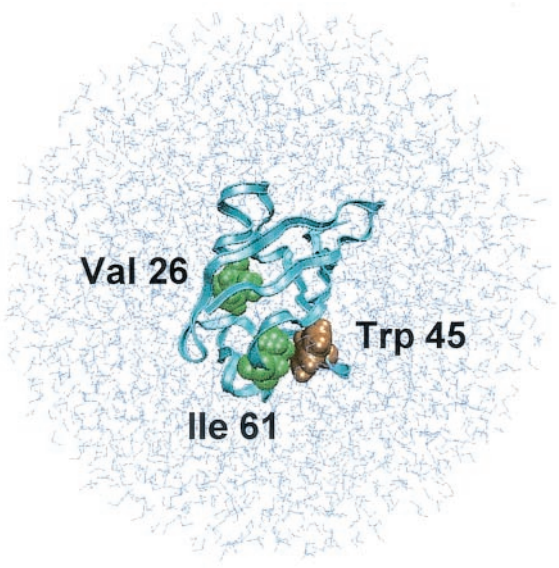

FIGURE 1 Ub*VI structure using the coordinates from Laub et al. (1995). Ile-61 is in van der Waals contact with Trp-45, whereas Val-26 has at least one intervening residue. Also shown is the extensive solvation shell used in the simulations.

EXPERIMENTAL METHODS AND RESULTS

In this section, we briefly review the preparation of the ubiquitin samples, as well as the fluorescence intensity and anisotropy measurements, which establish a correlation between fluorophore mobility and increased fluorescence intensity. The section concludes with the sample conditions for the apomyoglobin and phosphoglycerate kinase unfolding experiments.

Fluorescent ubiquitin and its cavity mutants

To perform our experiments, we chose various ubiquitin mutants as models for native states of differing flexibility. As a least-flexible reference molecule we select the fluorescent Phe-45-Trp variant of human ubiquitin, investigated extensively by Roder and coworkers (Laub et al., 1995). A structure of this variant, Ub*, with its single tryptophan residue is shown in Fig. 1. It is a mixed α/β protein with one α-helical segment and a short 3_{10} helical segment (Vijay-Kumar et al., 1987). Also shown in Fig. 1 are the two sites chosen in the protein core for mutation: Ile-61, which is in van der Waals contact with Trp-45, and Val-26, which has at least one intervening residue to Trp-45. The 61 site serves

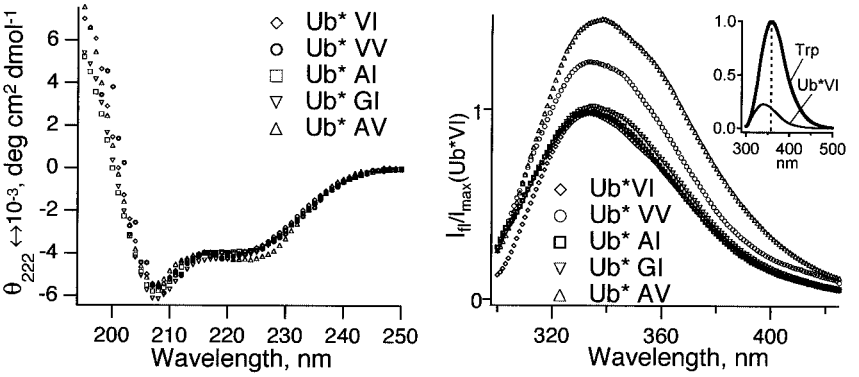

FIGURE 2 (*a*) Circular dichroism spectrum of the ubiquitin mutants used in this study (pH 5.9, 40 mM phosphate, 25°C). The CD spectra reveal only minor structural changes. (*b*) Fluorescence spectra show dramatic intensity increases for mutants that have a cavity near Trp-45. The insert shows that the folded pseudo wild-type Ub*VI has considerably smaller quantum yield than free tryptophan.

as an example for a site in which side chain truncation produces a cavity adjacent to the Trp, directly increasing the potential for fluorophore mobility, whereas position 26 is an example for a site that has an indirect effect on fluorophore mobility. The mutants represent various combinations of sidechain truncations at positions 26 and 61 and are summarized in Table 1; we use the abbreviation Ub*XY, in which X is the 26, and Y is the 61 position. All mutations replace simple aliphatic side chain residues with shorter aliphatic side chain residues. This avoids direct effects on the tryptophan fluorescence quenching via introduction or elimination of electron transfer, proton transfer, or Förster mechanisms. For this reason sites such as Tyr-59 or His-68 (3 Å and 5 Å distance to the Trp van der Waals surface, respectively) were not mutated: they contribute to the tryptophan quenching in the native state. Rather, changes in fluorescence intensity are due to small structural shifts or increased structural fluctuations, which occur as a consequence of the cavities and which affect either the tryptophan, its quenchers, or the protein as a whole.

The ubiquitin plasmid for site-directed mutagenesis was provided by the Handel group (Lazar et al., 1997). The protein was over-expressed in *Escherichia coli* (BL21), and the soluble fraction was purified using a method similar to that described in the literature (Lazar et al., 1997). The lyophilized protein was verified to be Ub* by low-resolution electrospray mass spectrometry and sodium dodecyl sulfate-polyacrylamide gel electrophoresis. Final buffer conditions used in all experiments were pH 5.9 in 40 mM phosphate at 25°C with varying amounts of guanidinium hydrochloride (GuHCl), as indicated. Mutants were generated using the Stratagene QuickChange kit, and purified and lyophilized like the wild type. Protein concentrations were measured to 3% by absorbance of the denatured proteins at 280 nm (Edelhoch 1967), using the fact that all mutants contain the same tryptophan, tyrosine, and phenylalanine residues in the same positions, and that positions 45 and 26 are not adjacent to 45 in sequence. Protein concentrations were in the range 10 μM (CD) to 170 μM (fluorescence anisotropy).

Circular dichroism

CD spectra and CD GuHCl titrations were used to verify that the native structure and folding cooperativity of the mutants are very similar to Ub*. The steady-state CD spectra are shown in Fig. 2 *a*. They are practically indistinguishable within the 3% experimental uncertainty imposed by concentration determinations, which indicates that the native structure of Ub* is at most slightly affected by the mutations. CD titrations were fitted to two-state models with a linear free energy dependence on denaturant $\Delta G(d) = \Delta G_0 + m \cdot d$ simultaneously with the fluorescence titrations (see below), confirming the two-state nature of all the unfolding transitions (Fig. 3). The free energies of folding are of course less negative for mutants with larger cavities (Table 1). CD was also measured at 280 to 300 nm, and the signal decreased smoothly with increasing GuHCl titration, supporting the notion of a less chiral sidechain environment for the aromatic residues (data not shown).

TABLE 1 Parameters for the ubiquitin mutants used in this study

Mutant	Abbreviation	ΔG, kJ/mol	RIF	RMS, Å 298 K	RMS, Å 400 K
Pseudo-WT	Ub*VI	−34 ± 1.5	1.00	1.2 ± 0.2	–
Ile-61-Val	Ub*VV	−18 ± 1	1.40	1.0 ± 0.1	1.7 ± 0.2
Val-26-Ala	Ub*AI	−20 ± 1.5	1.05	1.0 ± 0.1	1.3 ± 0.1
Val-26-Gly	Ub*GI	−4.9 ± 1.5	1.09	–	–
Val-26-Ala/Ile-61-Val	Ub*AV	−14 ± 1	1.70	1.0 ± 0.1	–

ΔG is the folding free energy at 0 M GuHCl, 25°C, pH 5.9 in 40 mM phosphate; RIF is the relative integrated fluorescence intensity compared with the pseudo wild type, RMS is the RMS fluctuation in the MD runs.

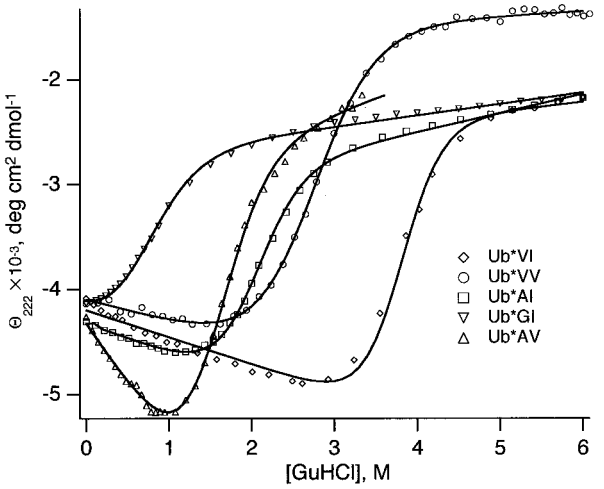

FIGURE 3 CD titration curves for several ubiquitin mutants. Without denaturant the mutants present similar amount of α-helix structure. Mutations at position 61 reduce the residual α-helix content at large GuHCl concentration. The free energies derived from the two-state fits (*lines*) are given in Table 1.

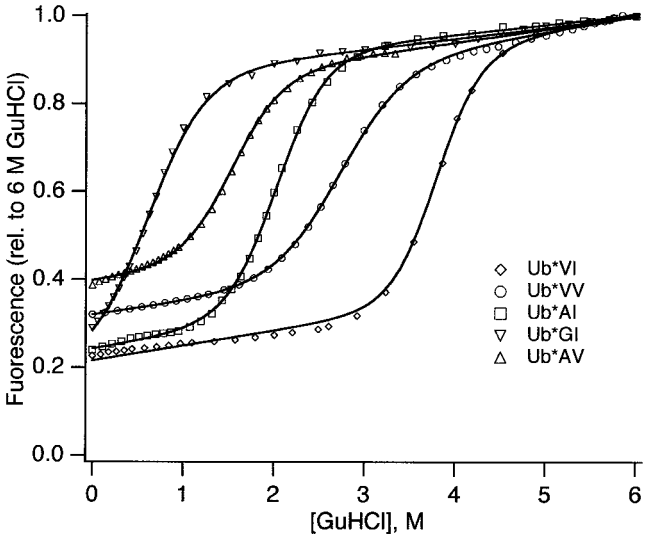

FIGURE 4 Fluorescence titration curves for several ubiquitin mutants. At 6 M GuHCl the fluorescence intensity observed was the same for all the mutants. At 0 M GuHCl the emission intensities for mutants with the Ile-61-Val mutation are larger, as shown in Fig. 2 *b*. The solid lines are two-state fits. All folded and all unfolded baselines were constrained to be equal, and the thermodynamic parameters were fitted simulatenously with the CD in Fig. 3 to minimize adjustable parameters.

Fluorescence

Fluorescence spectra were collected from 300 to 475 nm with 295-nm excitation and 0.5-nm resolution and corrected for aqueous Raman peaks. The steady-state fluorescence spectra of the unfolded proteins (6 M GuHCl) were found to be identical within measurement error. That was not the case for the fluorescence spectra of the folded proteins at 0 M GuHCl, as shown in Fig. 2 *b* and Table 1. Spectra fall into three classes: Ub*VI (pseudo wild type), Ub*AI (noncontacting cavity mutant), and Ub*GI (larger noncontacting cavity), whose fluorescence intensities are very similar or very slightly increasing in that order; Ub*VV (contacting cavity), which has a markedly higher fluorescence intensity; finally Ub*AV (both cavities) with fluorescence intensity higher still. Clearly, cavities not in contact with the tryptophan residue, even fairly nonconservative ones like the Val-26-Gly mutation, have little effect on the fluorescence intensity by themselves. Cavities in contact with the tryptophan lead to a significantly enhanced fluorescence intensity, which is further enhanced by the presence of additional cavities.

The quantum yield of Ub*VI (11 μM) relative to free Trp (3 μM solution) was determined to be 0.21 $\pm$ 0.05. The insert in Fig. 2 (right) illustrates this by comparing the fluorescence wavelength spectra on the same relative scale and also shows the blue-shift of all Ub spectra compared with free Trp, indicating significant burial of the fluorophore. The absolute quantum yield is therefore $<$0.04 for the pseudo-wild type. This indicates the presence of significant quenching in the native state, which is important because our proposed model (see Discussion) would not predict hyperfluorescence in proteins, which are not significantly quenched in the native state.

Fluorescence titrations were obtained by exciting at 295 nm and integrating over the 320- to 475-nm region. The titrations in Fig. 4 reveal the same effect as the 0 M GuHCl spectra: no difference in denatured fluorescence, markedly increased native fluorescence of the cavity mutants, particularly those with a Val adjacent to the fluorophore. The main additional information lies in the differing protein stabilities (Table 1). Fig. 4 shows simultaneous least squares fit with the CD titrations in Fig. 3, confirming cooperative two-state behavior by two different spectroscopic techniques. We note that Ub*GI has not leveled off at 0 M GuHCl, and a small amount of nonnative population may in fact be responsible for the slightly higher observed "native" fluorescence of this least stable of the mutants.

Fluorescence anisotropy

To correlate fluorescence intensity with enhanced tryptophan mobility, we measured the fluorescence anisotropy from 275 to 295 nm. The absolute anisotropy of Ub*VI and the relative fluorescence anisotropies of the cavity mutants are shown in Fig. 5. At 295 nm, where tryptophan excitation dominates, the anisotropies of Ub*AI and Ub*GI (noncontacting cavities) are nearly indistinguishable from Ub*VI; the anisotropy of the Ub*VV mutant (contacting cavity) is markedly lower; and the anisotropy of the Ub*AV mutant is lower still. This trend correlates perfectly with that observed in the fluorescence intensities: enhanced mobility of the

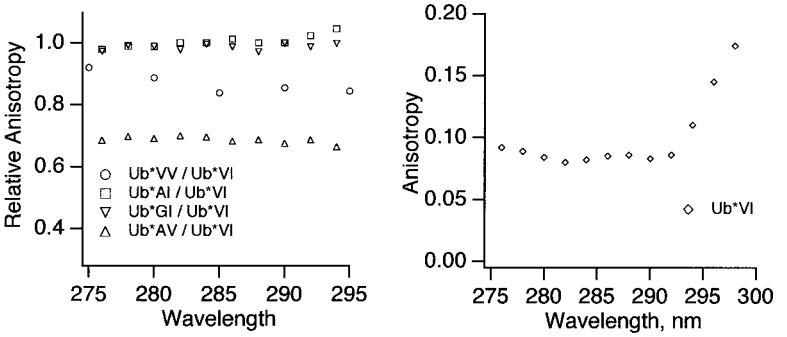

FIGURE 5 Anisotropy measurements at 25°C for ubiquitin mutants. The left panel shows the anisotropy ratio to the pseudo wild-type Ub*VI. Proteins with mutation Ile-61-Val have significantly smaller anisotropy, and thus have a more flexible Trp residue. The right panel presents the absolute anisotropyy data for the pseudo wild-type Ub*VI as a function of wavelength.

fluorophore in the native state corresponds to increased fluorescence intensity. To provide a bench mark for a wholly unfolded chain, we also measured the anisotropy for the Ub*AI mutant in 3 M GuHCl relative to Ub*VI in 0 M GuHCl and found it to be 0.38 ± 0.02, considerably lower than all the others observed in Fig. 5, and compatible with random orientation.

Hyperfluorescent proteins

To illustrate the mechanism with actual hyperfluorescent unfolding transitions, we studied two additional proteins: apomyoglobin (apoMb) denatured by GuHCl titration and phosphoglycerate kinase (PGK) by cold denaturation. Equine apomyoglobin was made from myoglobin (Sigma, St. Louis, MO; no further purification) by a modified acetone-acid extraction (Fanelli et al., 1958). Heme contamination by Soret band absorption was <1% for all samples. All GuHCl titrations were made in 40 mM phosphate buffer at pH 5.9 with protein concentration at 10 μM (CD) or 50 μM (fluorescence). Two types of PGK were studied: wild-type yeast PGK (yPGK was made using the yeast expression system developed by R. A Hitzeman at Genentech, and provided to us by M. Mas (Mas et al., 1986). A bacterially expressed His-tagged variant (hisPGK) was built by inserting the PGK gene into pET28 with a His-tag sequence and expressing in BL21codon+RP cells. His-tagged proteins were purified on a Ni-NTA column. yPGK and hisPGK were buffered in 20 mM phosphate, 0.1 M GuHCl, 1 mM EDTA, 1 mM dithiothreitol at pH 6.2 for all experiments. The CD spectra of yPGK and hisPGK were identical within measurement error. Cold denaturation scans by CD at 222 nm between −16°C and 10°C were found to be reversible. Cold denaturation was also detected by integrated fluorescence excited at 295 nm as detailed in Discussion.

COMPUTATIONAL METHODS AND RESULTS

We performed full atom, explicit solvent molecular dynamics simulations on Ub*VI and on the mutants derived from it to further test Trp mobility in these proteins. Molecular dynamics (MD) simulation provides an independent assessment of protein flexibility. Although the current generation of force fields is too harmonic for bending and stretching modes and might underestimate fluctuations in a packed native protein where such modes could contribute, one would nevertheless expect increased fluctuations, at least at elevated temperature or with the larger cavities, to confirm the trend observed by the fluorescence anisotropy measurements. MD simulations can also provide an invaluable measure of increases in overall protein flexibility, which cannot be accessed by the experiments.

MD simulations for the present problem must extend at least into the nanosecond time scale for two reasons. First, the nuclear magnetic resonance structure of Ub*VI was used as a starting point, and mutants derived from it in silico must be sufficiently relaxed into their native structures. Second, tryptophan fluorescence occurs on a nanosecond time scale, and so processes up to the nanosecond timescale can affect the fluorescence intensity and anisotropy homogeneously. It is also possible that much longer time scale inhomogeneous processes could affect the fluorescence, e.g., the mutants with cavities might have more microstates in the protein's energy landscape due to the increased entropy. Such inhomogeneous effects are not probed by the present MD simulations, but one would expect them to be greater in the cavity mutants.

To perform MD simulations of Ub*VI and its mutants, coordinates were taken from Laub et al. (1995). Minimization, equilibration, and MD runs for analysis were carried out using NAMD2 and the force field Charm22 (Brooks et al., 1983; Laxmikant et al., 1999). Results were visualized using the program VMD (Humphrey et al., 1996). Starting with the reported Ub*VI structure, mutations in silico were made using Insight II. The proteins were fully solvated using a sphere of TIP3 water molecules, covering the protein with at least five water layers (Fig. 1). The total number of atoms including the solvent was ~10,000. The energy of each system was first minimized at 0 K for 2 ps, and then equilibrated for 10 ps at 298 K. The systems Ub*VI, Ub*AI, Ub*VV, Ub*AV, Ub*AA, and Ub*VF were then simulated for 2 ns at 298 K. For additional simulations at 400 K, the last coordinate set from the corresponding 2-ns run was equilibrated at 400 K for 7 ps, then a MD run of 100 ps was

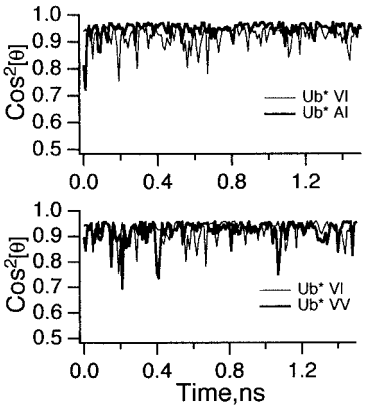

FIGURE 6 Fluctuation of tryptophan as function of time obtained from molecular dynamics simulations using NAMD at 298 K. The top panel compares the single mutant Ub*AI with the pseudo wild-type Ub*VI, whereas the bottom panel compares Ub*VV to Ub* VI. At 298 K, the AI mutant shows no significant increase in mobility, and the VV mutant shows a slight increase with the Charm22 force field.

performed to further equilibrate the system. Finally, 600-ps production runs at 400 K were made for Ub* AI and Ub* VV, the noncontacting cavity and contacting cavity mutants. From all of these trajectories 200 coordinate sets were collected, evenly spaced in time.

To monitor the fluctuation of the Trp residue relative to the backbone of the entire protein, the 200 snapshots were used to evaluate $\langle \cos^2\theta(t)\rangle$ as follows. One of the snapshot was chosen as a reference, and its backbone was fitted to the remaining 199 by rigid rotation and translation using Xplor (Brunger 1992); after these matches the projection $\cos\theta$ of the long axis of Trp for the reference snapshot onto all other 199 snapshots was calculated. The 199 projections were finally averaged as $\langle \cos^2\theta\rangle$ and plotted. This procedure was repeated selecting each of the remaining coordinate sets as the reference making maximum use of the single trajectories obtained in the simulations.

The results for MD simulations at 298 K suggest that the Ub*AI single mutation does not increase flexibility, whereas the Ub*VV single mutation (cavity near Trp-45) causes a small enhancement of tryptophan mobility (Fig. 6). This is the expected trend but on a much smaller scale than observed experimentally. In contrast, when position 26 is mutated in addition to a preexisting Ile-61-Val mutation, flexibility of the tryptophan greatly increases (Fig. 7). This by itself does not finger the "contact cavity" as the predominant source for enhanced tryptophan mobility because only both cavities together show greatly enhanced mobility.

The situation is quite different at 400 K (Fig. 8). There the "noncontacting cavity" mutant Ub*AI still has no significantly enhanced mobility compared to Ub*VI, but the "contacting cavity" mutant Ub*VV shows an enhanced mobility quite comparable with experiment. The trend here is exactly the same as observed experimentally: a cavity near the Trp residue most effectively enhances its mobility. We take all of these observations together as an indication that the force field used is slightly too rigid to detect the mobility differences seen by experiment at 298 K, but that they are observed at the higher temperature.

We also used the MD simulations to probe overall protein flexibility, as summarized in Table 1 by the root mean square atomic deviations or mean Debye-Waller factors for the 200 runs. The overall flexibility of Ub*VI and its mutants is comparable at 298 K. The root mean square deviation increases significantly at 400 K. Notably, it increases much faster for the Ub*VV mutant than for the Ub*AI mutant: in addition to local cavity effects, the former

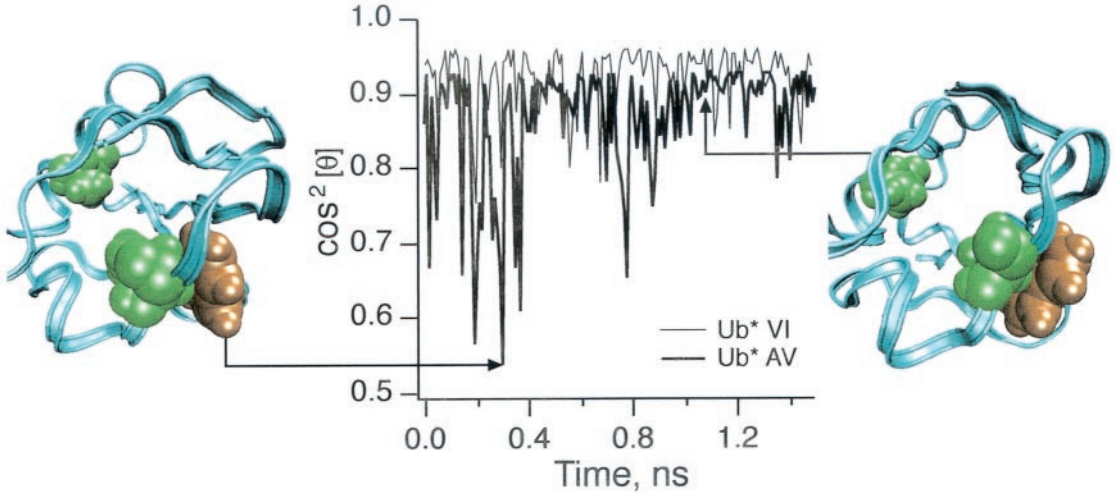

FIGURE 7 MD simulation of tryptophan fluctuations at 298 K. The double mutant has a more flexible tryptophan compared with the pseudo wild type. The insert panels show the Trp environment at small and large displacements from the average structure.

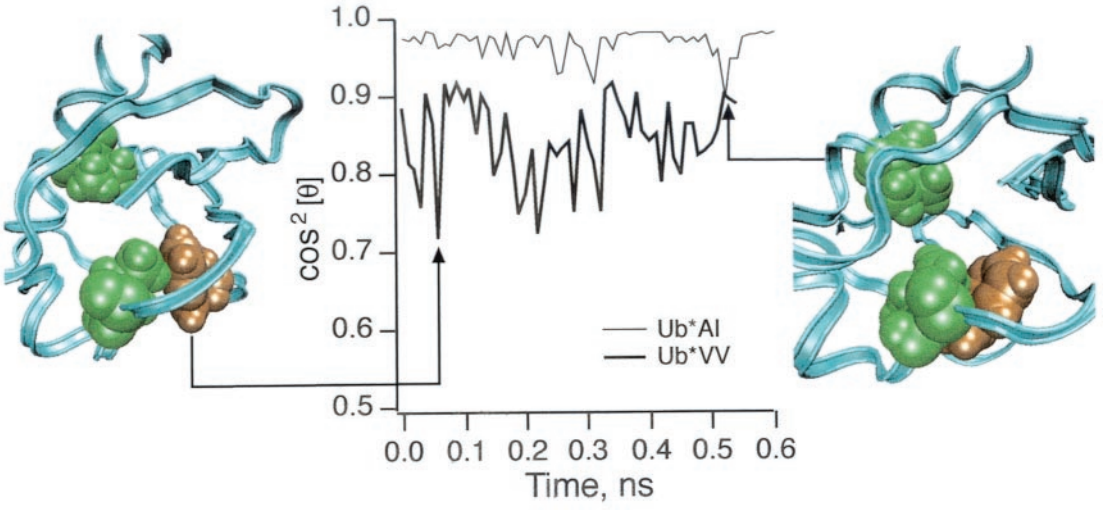

FIGURE 8 MD simulation at 400 K for the single mutants Ub* VV and Ub* AI. At this temperature the protein with a void near to tryptophan has significantly higher fluorophore mobility than the protein with a cavity not in contact with the fluorophore. The insert panels show the local Trp environment at a small and at a large displacement from the average structure.

mutation also enhance overall protein flexibility, thereby contributing even further to the mobility of the fluorophore.

DISCUSSION

The results in the previous two sections establish a strong correlation between increased tryptophan mobility and increased tryptophan fluorescence intensity in native proteins with quenched tryptophan fluorophores. The Ub*VV mutant, with the cavity near the fluorophore, has 20% lower anisotropy and 40% higher integrated fluorescence intensity than either the pseudo wild type or the Ub*AI/GI mutants with noncontacting cavities. The fluorescence intensity is increased by 70%, and the anisotropy further decreased when a second cavity is added, even if that cavity is not in contact with the fluorophore and has little effect on its own. Increases of 40% to 70% in fluorescence intensity are in the range of hyperfluorescence observed during unfolding titrations of proteins (see examples below). The magnitude of the effects observed here is therefore easily capable of explaining hyperfluorescence as a pretransition increase in fluorophore mobility caused by enhanced native state flexibility.

We now propose a model for the relationship between conformational flexibility and hyperfluorescence (or other fluorescence properties). The proposed mechanism invokes both static (heterogeneous) and dynamic (homogeneous) effects of the protein conformational distribution on fluorescence. It explains the observed features of hyperfluorescence. The model draws on the idea of gated electron transfer reactions (Hoffman et al., 1991), which in turn are related to dynamical narrowing familiar from protein folding studies by magnetic resonance spectroscopy (Huang and Oas, 1995). The general scheme is outlined in Fig. 9.

Native tryptophan fluorescence is very sensitive to the conformational environment of the fluorophore. Lifetimes (typically 1–5 ns), quantum yields (typically 0.05–0.2), and intensities all depend on the disposition of quenchers and fluorophore in the protein conformational substates (Gilst et al., 1994; Grinvald and Steinberg, 1976; Kirby and Steiner, 1970). Prime quenching candidates in ubiquitin are Tyr-59 (3 Å van der Waals distance to Trp-45) and His-68 (5 Å). Quenching in apoproteins usually occurs via excited state electron transfer or proton transfer (Chen and Barkley, 1998; Gilst et al., 1994; Steiner and Kirby, 1969). The lifetime and quantum yield of tryptophan fluorescence are generally controlled by the quenching rate. The quenching rates of conformational substates differ widely. Only a small fraction of substates has the highest Franck-Condon overlaps for rapidly converting excited Trp* to the ionized or protonated quenched state Trp^q. The fraction of most strongly quenched substates is small because of the exponential distance dependence of proton and electron transfer processes.

In the scheme shown in Fig. 9, the fluorophore is initially in the ground state. An ensemble $\{C_i\}$ of conformational substates is populated (Frauenfelder et al., 1991). The ensemble is broader in a flexible native state near the unfolding transition. Next, the tryptophan is excited to an ensemble $\{C_i^*\}$. The electronic transition is sudden compared with the conformational time scales of the backbone and side chains, preserving the ground state distribution immediately after excitation. Thus, a more flexible native protein leads to a broader conformational distribution of excited states. Now

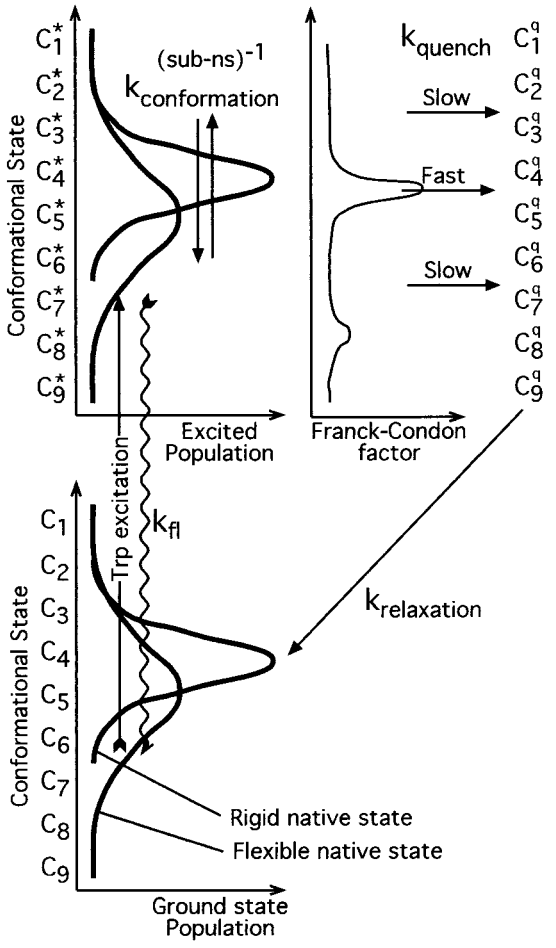

FIGURE 9 Static and dynamic relaxation mechanisms for enhanced tryptophan intensity. (*Bottom*) Before excitation, the more flexible native state has access to a wider range of conformational states. (*Top*) After excitation, this diversity is preserved. Because the quenching mechanism is fastest for only a small ensemble of conformations (*top middle*), fluorescence will either increase in the broader conformational ensemble or decrease only very slightly if the broader ensemble already samples the majority of less quenched states (static mechanism). In addition, conformational interchange (*curved arrow*) on the same time scale as fluorescence quenching can lead to motional narrowing and dilute the effect of gateway states, further enhancing the fluorescence intensity (dynamic mechanism).

two things happen: conformational ensembles can interconvert with rate constants $k_{\text{conformation}}$, and they can decay to the quenched ensemble $\{C_i^q\}$ with rate constants k_{quench} that depend on the conformational state (Bismuto and Irace, 1994; Petrich et al., 1983; Wu and Brand, 1994). k_{quench} determines the population left in $\{C_i^*\}$ and hence the fluorescence properties.

If the narrow native conformational ensemble happens to have a large Franck-Condon overlap for quenching, broadening the ensemble (by adding cavities or by stressing the protein during a denaturation titration) will result in a large increase in fluorescence because many new substates with smaller Franck-Condon factors are accessed. The converse is not true, unless the interconversion rate is too high, because the majority of conformational substates are ineffective at quenching; only a small decrease in fluorescence intensity would be expected when an unquenched ensemble broadens and overlaps a few fast quenching channels. Our model naturally explains the absence of "hypofluorescence." Only proteins with significantly quenched native states can hyperfluoresce in this model because hyperfluorescence results from a reduction of quenching induced by increased fluorophore mobility. Ub*VI falls into this class (Fig. 2), and so do others, but not every two-state folder will hyperfluoresce.

This "static" picture is further enhanced by the "dynamic" interconversion among the $\{C_i\}$ with rate constants $k_{\text{conformation}}$. When only a few conformational states are quenched with the maximal possible efficiency, conformational averaging closes their "gate" to $\{C_i^q\}$, but only slightly opens the gate for the majority of weakly quenched conformations. This picture has been worked out quantitatively by (Hoffman et al., 1991). The MD simulations are also suggestive of such a conformational interconversion contribution to hyperfluorescence because the fluctuations in Figs. 7 and 8 occur on a timescale somewhat faster than the fluorescence lifetime of ≈2.5 ns, which we determined for Ub*VI. This conformational timescale has also been determined by phase fluorimetry (Lakowicz and Cherek, 1980). This suggests that hyperfluorescence could be used as a tool to study conformational interconversion.

The model in Fig. 9 explains all the observed features of hyperfluorescence when it is concurrent with two-state behavior by other spectroscopic techniques. Only some unfolding transitions, which are two state by other techniques (e.g., CD) exhibit hyperfluorescence. Hypofluorescence is generally not observed. Increased fluorescence is observed when the tryptophan environment becomes more flexible, as in our Ub* experiments. Hyperfluorescence is usually observed in the middle of the two-state transition as determined by CD or other methods. This is where the population of the pretransition flexible native state reaches a maximum. Hyperfluorescence of a fluorophore is only observed when its native fluorescence quantum yield is fairly low.

Increased conformational flexibility also affects other fluorescence observables, such as the anisotropy. For example, our model predicts that increased conformational flexibility should be accompanied by a decrease in anisotropy, whereas the native state is still populated. This would be followed by a second stage of decrease in which the loosened native state interchanges with the unfolded state near $K_{\text{eq}} \approx 1$.

We finally consider two cases in which hyperfluorescence has been observed during protein unfolding titrations and which are perhaps better described by a loosened pretransition native ensemble. The first of these involves the GuHCl-induced denaturation of apomyoglobin at pH 6.

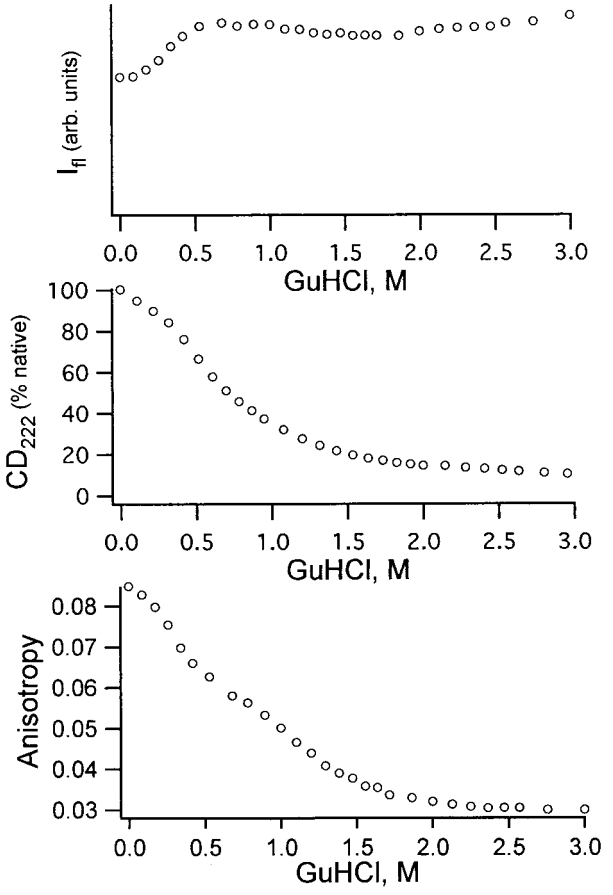

FIGURE 10 GuHCl denaturant titration of horse apomyoglobin at pH 5.9. The upper panel shows the relative fluorescence intensity, which exhibits a hyperfluorescence peak. The middle panel presents the fraction of α-helical structure monitored by CD, which is two-state like. The lower panel shows the anisotropy, which measures the mobility of the tryptophan residues.

Chemical denaturation of apomyoglobin have been extensively studied. A thermodynamic intermediate visible by both CD and fluorescence is populated at pH 4 (Barrick and Baldwin, 1993; Griko et al., 1988; Kay and Baldwin, 1996; Kirby and Steiner, 1970). The same GuHCl titration studies at pH 6 show little population of this intermediate by CD (Barrick and Baldwin, 1993), yet there still is hyperfluorescence. Our own CD, fluorescence intensity, and fluorescence anisotropy measurements corroborate these findings for chaotropic denaturation (Fig. 10). The fluorescence intensity is significantly nonmonotonic, anisotropy shows a rapid initial decline, but the CD spectrum is two-state like. The hyperfluorescence maximum falls near the midpoint of the two-state CD curve and of the fluorescence anisotropy decay, suggesting that the hyperfluorescence is associated with a native state, which has enhanced conformational flexibility during the two-state transition to the unfolded state.

The second example is summarized in Fig. 11. The 415-residue, two-domain protein yeast phosphoglycerate kinase (yPGK) (Missiakas et al., 1990) undergoes cold denaturation between 0 and −20°C (Gast et al., 1993). The CD signals of yPGK at 222 and 295 nm are well fitted by a two-state transition, yet the fluorescence intensity shows marked hyperfluorescence. We constructed a hisPGK variant, which differs only by the attachment of a 20-residue (histidine+thrombin cleavage site) tag at the N terminus. The CD spectrum of this variant is also two-state like, although it cold denatures slightly more than yPGK (Fig. 11). Unlike yPGK, hisPGK has no hyperfluorescence (only a small enhancement of fluorescence intensity in the transition region remains). One could rationalize these results with the following (not very satisfying) explanation: the His tag has little effect on native stability, yet thoroughly destabilizes a presumed folding intermediate seen in yPGK, which just happens to be unobservable by CD. The following explanation seems more likely that such a tag affects the conformational flexibility of the native state on the verge of unfolding, especially since its 20-residue length is sufficient to interact with the C-terminal domain, while the CD spectrum monitors the two-state transition.

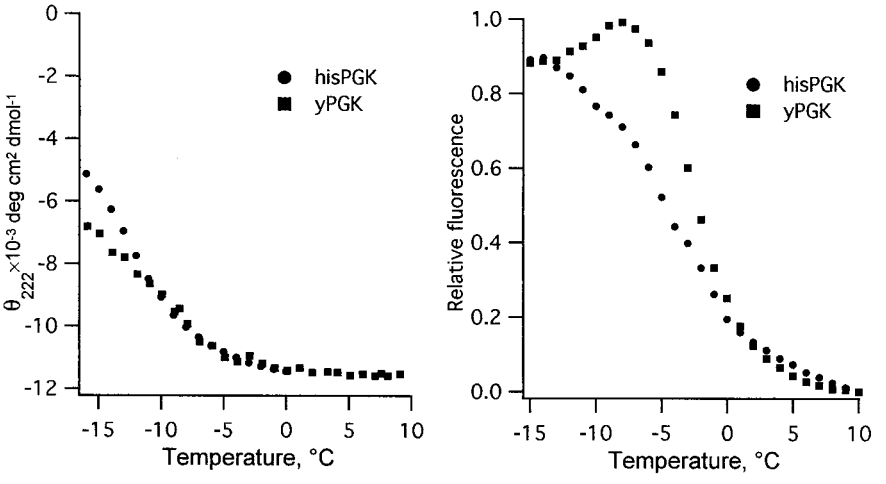

FIGURE 11 Temperature-scan of yPGK and hisPGK monitored by CD and fluorescence intensity. Introduction of the His tag does not shift the onset of cold denaturation, which still appears two state-like by CD, but greatly reduces the hyperfluorescence observed in yPGK.

Increased static or dynamic conformational heterogeneity of the native state during unfolding provides a reasonable alternative to folding intermediates for explaining hyperfluorescence. Enhanced tryptophan mobility and increased fluorescence intensity are clearly correlated in native-like protein molecules, as shown by our study of ubiquitin. Furthermore, there are cases where deviations from two-state folding are evident only by fluorescence not by other probes of unfolding. These facts should lead one to be cautious about interpreting nonmonotonic fluorescence of proteins during unfolding titrations as firm evidence for folding intermediates. Instead, several spectroscopic techniques, including some not sensitive to side chain mobility, should be used to investigate the unfolding, and corroborate multistate folding.

This work was supported by grants from the National Institutes of Health R01 GM057175 (to M.G.), from the National Institutes of Health P41 RR05969-04 (to K.S.), as well as by a computer time grant of the National Science Foundation RCA 935028 (to K.S.). Edgar Larios was recipient of a Beckman Institute Graduate Fellowship while this work was carried out. The authors thank the UIUC Theoretical Biophysics Group where simulations were carried out, and the National Institutes of Health-supported UIUC Laboratory for Fluorescence Dynamics where the anisotropy measurements were made.

REFERENCES

Baker, D. 2000. A surprising simplicity to protein folding. *Nature.* 405: 39–42.

Barrick, D., and R. Baldwin. 1993. Three-state analysis of sperm whale apomyoglobin folding. *Biochemistry.* 32:3790–3796.

Beechem, J. M., M. A. Sherman, and M. T. Mas. 1995. Sequential domain unfolding in phosphoglycerate kinase: fluorescence intensity and anisotropy stopped-flow kinetics of several tryptophan mutants. *Biochemistry.* 34:13943–13948.

Bismuto, E., and G. Irace. 1994. Unfolding pathway of apomyoglobin simultaneous characterization of acidic conformational states by frequency domain fluorometry. *J. Mol. Biol.* 241:103–109.

Brooks, B. R., R. E. Bruccoleri, B. D. Olafson, D. J. States, S. Swaminathan, and M. Karplus. 1983. CHARMM: a program for macromolecular energy, minimization, and dynamics calculations. *J. Comput. Chem.* 4:187–217.

Brunger, A. T. 1992. X-PLOR: A System for X-Ray Crystallography and NMR. Yale University Press, New Haven, CT.

Callis, P., and T. James. 2001. Mechanisms of tryptophan fluorescence shifts in proteins. *Biophys. J.* 80:2093–2109.

Chen, Y., and M. D. Barkley. 1998. Toward understanding tryptophan fluorescence in proteins. *Biochemistry.* 37:9976–9982.

Edelhoch, H. 1967. Spectroscopic determination of tryptophan and tyrosine in proteins. *Biochemistry.* 6:1948–1954.

Fanelli, A. R., E. Antonini, and A. Caputo. 1958. Studies on the structure of hemoglobin I. *Physicochem. Prop. Hum. Globin. Methods Enzymol.* 30:608–615.

Frauenfelder, H., S. G. Sligar, and P. G. Wolynes. 1991. The energy landscapes and motions of proteins. *Science.* 254:1598–1603.

Gast, K., G. Damaschun, H. Damaschun, R. Misselqitz, and D. Zirwer. 1993. Cold denaturation of yeast phophoglycerate kinase: kinetics of changes in secondary structure and compactness on unfolding and refolding. *Biochemistry.* 32:7747–7752.

Gilst Mv, C. Tang, A. Roth, and B. Hudson. 1994. Quenching interactions and nonexponential decay: tryptophan 138 of bacteriophage T4 lysozyme. *J. Fluoresc.* 4:203–207.

Gomez, J., V. J. Hilser, D. Xie, and E. Freire. 1995. The heat-capacity of proteins. *Proteins.* 22:404–412.

Griko, Y. V., P. L. Privalov, S. Y. Venyaminov, and V. P. Kutyshenko. 1988. Thermodynamic study of the apomyoglobin structure. *J. Mol. Biol.* 220:127–138.

Grinvald, A., and I. Z. Steinberg. 1976. The fluorescence decay of tryptophan residues in native and denatured proteins. *Biochim. Biophys. Acta.* 427:663–678.

Gruebele, M. 1999. The physical chemistry of protein folding. *Ann. Rev. Phys. Chem.* 50:485–516.

Gruebele, M. 2002. Protein folding: gauging the free energy surface. *Curr. Opin. Struct. Biol.* 12:161–168.

Hoffman, B. M., M. A. Ratner, and S. A. Wallin. 1991. Energetics and dynamics of gated reations. *In* Electron Transfer in Inorganic, Organic, and Biological Systems. J. R. Bolton, N. Mataga, G. McLendon, editors. American Chemical Society, Washington, DC. 125–146.

Huang, G. S., and T. G. Oas. 1995. Submillisecond folding of monomeric λ repressor. *Proc. Natl. Acad. Sci. U. S. A.* 92:6878–6882.

Hudson, B. S., J. M. Huston, and G. Soto-Campos. 1999. A reversible "dark state" mechanism for complexity of the fluorescence of tryptophan in proteins. *J. Phys. Chem. A.* 103:2227–2234.

Humphrey, W. F., A. Dalke, and K. Schulten. 1996. VMD visual molecular dynamics. *J. Mol. Graph.* 14:33–38.

Jennings, P., and P. Wright. 1993. Formation of a molten globule intermediate early in the kinetic folding pathway of apomyoglobin. *Science.* 262:892–895.

Kay, M., and R. Baldwin. 1996. Specific packing in apomyoglobin molten globule. *Nat. Struct. Biol.* 3:439–445.

Khorasanizadeh, S., I. Peters, and H. Roder. 1996. Evidence for a three-state model of protein folding from kinetic analysis of ubiquitin variants with altered core residues. *Nat. Struct. Biol.* 3:193–205.

Kiefhaber, T., and R. L. Baldwin. 1995. Intrinsic stability of individual alpha helices modulates structure and stability of the apomyoglobin molten globule form. *J. Mol. Biol.* 252:122–132.

Kim, P. S., and R. L. Baldwin. 1990. Intermediates in the folding reactions of small proteins. *Ann. Rev. Biochem.* 59:631–660.

Kirby, E. P., and R. F. Steiner. 1970. The tryptophan microenvironments in apomyoglobin. *J. Biol. Chem.* 245:6300–6306.

Lakowicz, J. R., and H. Cherek. 1980. Dipolar relaxation in proteins on the nanosecond timescale observed by wavelength-resolved phase fluorometry of tryptophan fluorescence. *J. Biol. Chem.* 255:831–834.

Laub, P., S. Khorisanizadeh, and H. Roder. 1995. Localized solution structure refinement of an F45W variant of ubiquitin using stochastic boundary molecular dynamics and NMR distance restraints. *Protein Sci.* 4:973–982.

Laxmikant, K., R. Skeel, M. Bhandarkar, R. Brunner, A. Gursoy, N. Krawetz, J. Phillips, A. Shinozaki, K. Varadarajan, and K. Schulten. 1999. NAMD2: greater scalability for parallel molecular dynamics. *J. Comp. Phys.* 151:283–312.

Lazar, G. A., J. R. Desjarlais, and T. M. Handel. 1997. De novo design of the hydrophobic core of ubiquitin. *Protein Sci.* 6:1167–1178.

Mas, M. T., C. Y. Chen, R. A. Hitzeman, and A. D. Riggs. 1986. Active human-yeast chimeric phosphoglycerate kinases engineered by domain interchange. *Science.* 233:788–790.

Missiakas, D., J. Betton, P. Minard, and J. M. Yon. 1990. Unfolding-refolding of the domains in yeast phosphoglycerate kinase: comparison with the isolated engineered domains. *Biochemistry.* 29:8683–8689.

Onuchic, J. N., P. G. Wolynes, Z. Luthey-Schulten, and N. D. Socci. 1995. Toward an outline of the topography of a realistic protein folding funnel. *Proc. Natl. Acad. Sci. U. S. A.* 92:3626–3630.

Petrich, J. W., M. C. Chang, D. B. McDonald, and G. R. Fleming. 1983. On the origin of nonexponential fluorescence decay in tryptophan and its derivatives. *J. Am. Chem. Soc.* 105:3815–3832.

Postnikova, G. B., Y. E. Komarov, and E. M. Jumakova. 1991. Fluorescence study of the conformational properties of myoglobin structure 1: pH-dependent changes of tryptophanyl fluorescence in intact and chemically modified sperm whale apomyoglobins. *Eur. J. Biochem.* 198: 223–232.

Press, W. H., S. A. Teukolsky, W. T. Vetterling, and B. P. Flannery. 1992. Numerical recipes in FORTRAN: the art of scientific computing. Cambridge University Press, Cambridge, UK.

Privalov, P. L., N. N. Khechinashvili, and B. P. Atanasov. 1971. Thermodynamic analysis of thermal transitions in globular proteins: I. Calorimetric study of ribotrypsinogen, ribonuclease and myoglobin. *Biopolymers.* 10:1865–1890.

Ross, J. B. A., C. J. Schmidt, and L. Brand. 1981. Time-resolved fluorescence of the two tryptophans in horse liver alcohol dehydrogenase. *Biochemistry.* 20:4369–4377.

Sabelko, J., J. Ervin, and M. Gruebele. 1998. The cold denatured ensemble of apomyoglobin: implications for the early steps of folding. *J. Phys. Chem. B.* 102:1806–1819.

Seemann, H., R. Winter, and C. A. Royer. 2001. Volume, expansivity and isothermal compressibility changes associated with temperature and pressure unfolding of staphylococcal nuclease. *J. Mol. Biol.* 307: 1091–1102.

Shea, J. E., J. N. Onuchic, and C. L. Brooks I. 2000. Energetic frustration and the nature of the transition state ensemble in protein folding. *J. Chem. Phys.* 113:7663–7671.

Steiner, R. F., and E. P. Kirby. 1969. The interaction of the ground and excited states of indole derivatives with electron scavengers. *J. Phys. Chem.* 73:4130–4135.

Vijay-Kumar, S., C. E. Bugg, and W. J. Cook. 1987. Structure of ubiquitin refined at 1.8 Å resolution. *J. Mol. Biol.* 194:531–544.

Wu, P. G., and L. Brand. 1994. Conformational flexibility in a staphylococcal nuclease mutant K45C from time-resolved resonance energy transfer measurements. *Biochemistry.* 33:10457–10462.

Yeomans, J. M. 1992. Statistical mechanics of phase transitions. Clarendon Press, Oxford, UK. 1–153.